RSC Advances

PAPER

View Article Online
View Journal | View Issue

Cite this: *RSC Adv.*, 2018, **8**, 28953

Enhanced visible transmittance and reduced transition temperature for VO_2 thin films modulated by index-tunable SiO_2 anti-reflection coatings

Maodong Zhu,[ab] Hongji Qi,*[a] Bin Wang,[a] Hu Wang,[a] Dongping Zhang*[c] and Weizhong Lv[d]

The low visible transmission is one of the bottleneck problems for the application of vanadium dioxide films since the high refractive index (RI) of VO_2 films results in strong reflection in the visible wavelength. To address this problem, in this paper, high-purity VO_2 films were deposited on fused silica by DC reactive magnetron sputtering at low temperature of 320 °C. Silica sol–gel coatings with tunable refractive index (RI) coated onto VO_2 films have been fabricated to enhance visible transmittance with the potential application in the field of smart windows. SiO_2 coatings with tunable RI (1.16–1.42 at $\lambda = 700$ nm) were prepared by sol–gel dip-coating technique. The double structure SiO_2/VO_2 films were characterized through several techniques, including X-ray diffraction, UV-VIS-NIR spectrophotometry and scanning electron microscopy. Compared with the single-layer VO_2 film (ΔT_{sol} of 6.25% and T_{lum} of 38.58%), the three kinds of SiO_2/VO_2 bilayer films had higher T_{lum} (41.93–50.44%) and larger ΔT_{sol} (8.15–8.51%) simultaneously due to significantly decreased reflectance. Moreover, the crystallization properties of VO_2 films are essentially unchanged by applying a SiO_2 top layer, while the phase transition temperature and thermal hysteresis width of sample S116 are lower than those of pure VO_2 film. The presented RI-tunable SiO_2 coatings, can regulate optical properties continuously for various VO_2 substrates, paving the way for practical applications of VO_2 films in the field of smart windows or others.

Received 26th June 2018
Accepted 9th August 2018

DOI: 10.1039/c8ra05479g

rsc.li/rsc-advances

1. Introduction

Vanadium dioxide (VO_2) is the best thermochromic material for energy-efficient smart windows.[1,2] At the critical temperature (~68 °C), a reversible semiconductor-to-metal transition occurs in bulk VO_2.[3] Accompanied with the crystal structure transitioning from rutile phase (R) to monoclinic phase (M), VO_2 exhibits a drastic change in electrical conductivity and NIR optical transmittance.[4] Such specific features make VO_2 a potential candidate in the application of thermochromic energy-efficient smart windows, uncooled infrared (IR) microbolometers, laser protection and optical storage devices.[5–8] High-purity VO_2 films can be fabricated by many preparation methods, including the pulsed laser deposition, sol–gel method, chemical vapor deposition (CVD), thermal evaporation, atomic layer deposition and magnetron sputtering.[9–14] Among these, magnetron sputtering technology shows great advantages for the application of VO_2 films in smart windows due to the good uniformity and potential for industrialization.[15]

Up till now, there has been no successful application of vanadium dioxide in the field of smart windows. To realize an available solution, several challenges needed to be overcame: low solar modulating ability, unattractive color, high transition temperature and especially low visible transmittance. Generally, the low transmission of single 80 nm VO_2 film can only reach 40% in the visible region (380–780 nm).[16] There have been various popular methods to enhance the visible transmittance of VO_2 films: metal-ion doping,[17] multilayer structure,[18] porous texture,[19] *etc.* Moreover, VO_2 films with different nanostructures can behaver enhanced T_{lum} and ΔT_{sol}, such as moth eye structure,[20] photonic structure,[21] plasmonic structure[22] and grided structure[23]. Additionally, applying antireflection coatings (ARCs) on the film surface can also be a promising approach to improve the visible transmittance of VO_2 films through TiO_2, ZnO, ZrO_2 or SiO_2, *etc.*,[24] which is useful in industrial applications. The anti-reflective devise of double-layer films should be enhanced as the high RI and reflectivity of VO_2 films in the

[a]*Key Laboratory of Materials for High Power Laser, Shanghai Institute of Optics and Fine Mechanics, Chinese Academy of Sciences, Shanghai, 201800, China. E-mail: qhj@siom.ac.cn*

[b]*University of Chinese Academy of Sciences, Beijing, 100049, China*

[c]*Shenzhen Key Laboratory of Advanced Thin Film and Applications, College of Physics and Energy, Shenzhen University, Shenzhen, 518060, China. E-mail: zdpsiom@szu.edu.cn*

[d]*Shenzhen University, Shenzhen, 518060, China*

visible region. However, most of the overcoats are usually with high RI, expensive and energy-consuming. It is worth noting that compared with other antireflection coatings, the SiO_2 coatings with low RI prepared by low-cost sol–gel methods behaved some advantages of large-area, widespread used and anti-oxidation.[25,26] Much research has been devoted to the fabrication of SiO_2/VO_2 double-layer structure to improve the visible transmission of VO_2 films significantly. Yu *et al.* increased the T_{lum} of VO_2 film from 37.6% to 47.7% *via* SiO_2/VO_2 composite structure, while ΔT_{sol} exhibited an obvious decrease trend from 8.06% to 7.62%.[27] Zhang *et al.* introduced SiO_2 with RI of 1.299 as an antireflection coating coated on the VO_2 film, which improved the visible transmission from 69.8% to 80.0% significantly, whereas the NIR control capability was also slightly decreased from 12.6% to 10.2%.[28]

Therefore, in this study, SiO_2 anti-reflection coatings with tunable refraction index were coated on VO_2 films to enhance ΔT_{sol} and T_{lum} simultaneously and continuously. Furthermore, the RI tunability of top SiO_2 coatings can be applied to not only the VO_2 continuous thin films but also the nanocomposites and micro-patterned VO_2 films to improve the nano-thermochromism effect.[29] In addition, an anti-oxidation overcoat is also necessary for the unstable VO_2 films. Index-tunable anti-reflection SiO_2 coatings optimized by sol–gel method prepared on the surface of VO_2 films by sol–gel dip-coating technique. The effect of RI tunability of SiO_2 coatings on the thermochromism and optical properties of VO_2 films was investigated.

2. Experimental details

VO_2 films were deposited on the fused silica by reactive magnetron sputtering technique. The deposition chamber was pumped to a base pressure of 4×10^{-4} Pa by using a turbo molecular pump, and pre-cleaned in Ar gases for 10 min to remove contamination from the target surface. The vanadium target (Φ60 mm) of purity 99.999% was used and the power density of V target was 4.2 W cm^{-2}. The distance of target-substrate was approximately 100 mm. Pure oxygen gas and argon gas were introduced to chamber at 1.8 sccm and 40 sccm, respectively. The deposition pressure and substrate temperature were maintained at 0.5 Pa and 320 °C, respectively. The deposition time was 30 min and the thickness of VO_2 films was controlled accurately to 150 nm. A schematic of DC magnetron sputtering is shown in Fig. 1(a). For low refractive silica (n = 1.16), the SiO_2 sols were prepared by base catalysis of ammonia, mixed with the teraethoxysilane (TEOS), H_2O, NH_3 and ethanol (C_2H_5OH). The molar ratio of TEOS, H_2O, C_2H_5OH and NH_3 was

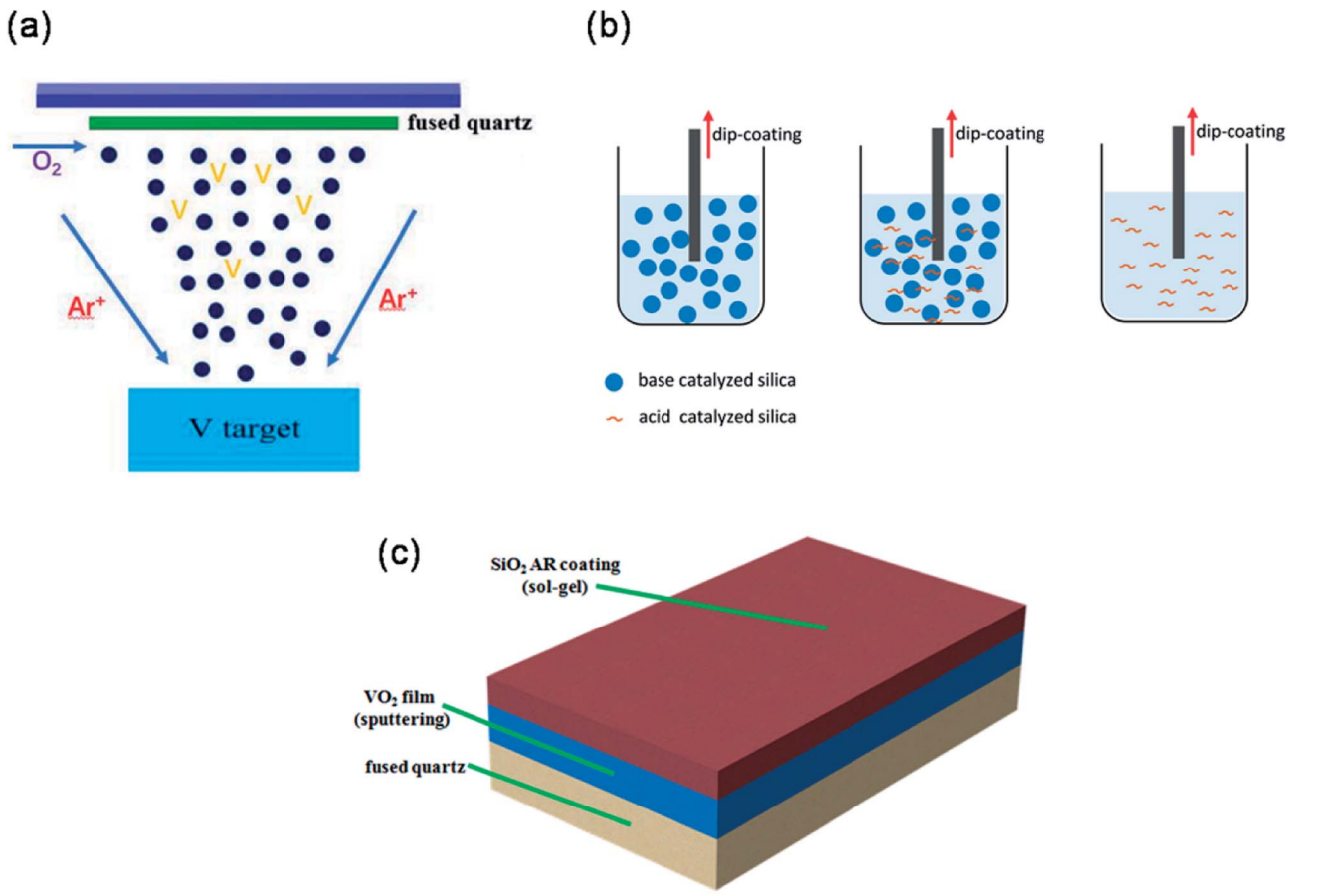

Fig. 1 Schematic diagrams of procedure of preparation of (a) VO_2 films and (b) SiO_2 sols. (c) Schematic illustration of the structure of SiO_2/VO_2 double-layer film.

1 : 2 : 34.2 : 0.9.[30] High refractive silica (n = 1.42) was synthesized by mixing teraethoxysilane (TEOS), H_2O, HCl and ethanol (C_2H_5OH). The molar ratio of TEOS, H_2O, C_2H_5OH and HCl was 1 : 4 : 20 : 0.05.[31] The SiO_2 coating with refractive index of 1.34 was prepared by mixing low refractive silica and high refractive silica with a molar ratio of 7 : 3.

The above resulting chemical reagents were stirred for 5 h and placed into an oven to age for 4 days. VO_2 films (Φ30 mm, d = 3 mm) were coated with the three kinds of silicas by a dip coating process with a withdrawal speed of 7 cm min^{-1}, and then were baked at 180 °C for 24 h. The thickness of SiO_2 antireflection coating was about 110 nm. The schematics of preparation process of SiO_2 sols and dip coating process are shown Fig. 1(b). The SiO_2/VO_2 bilayer films coated by SiO_2 coatings with refractive indices of 1.16, 1.34 and 1.42 are denoted as S116, S134 and S142, respectively. And the VO_2 film without SiO_2 antireflection is marked as PVO_2. Fig. 1(c) illustrates the structure of VO_2 film on fused quartz with a SiO_2 antireflection coating. The optical transmittance of the SiO_2/VO_2 bilayer films were studied with a PerkinElmer Lambda 950 UV-VIS-NIR spectrophotometer from 250 to 2500 nm. A spectroscopic ellipsometer (Horiba uvisel 2) was used to characterize the refractive indices and physics thickness of SiO_2 coatings. The microstructure characterization of pure VO_2 and SiO_2/VO_2 bilayer films was measured by X-ray diffraction (Rigaku Ultima IV) with a 2θ geometry. In addition, the optical transition behavior was studied by Thin film phase transition measurement system (PERFECT PTM1700) to collect the IR transmittance of films at a fixed wavelength (1550 nm) against temperature with an interval of 1.0 °C. The surface morphologies of the films were observed using a field-emission scanning electron microscope (Zeiss Supra 5S). The calculation of integral visible transmittance (T_{lum}, 380–780 nm) and solar transmittance (T_{sol}, 250–2500 nm) can refer to our previous work.[16]

3. Results and discussion

The refractive index of SiO_2 films with wavelength were measured by using ellipsometry and fitted by Cauchy ellipsometry model. Fig. 2 shows the refractive indices of SiO_2 antireflection coatings dipped by base catalyzed silica, acid catalyzed silica and mixed of them on the fused quartz. The refractive index of the SiO_2 film prepared by base catalyzed silica was measured to be ~1.16 at 700 nm, considerably lower than that prepared by acid catalyzed silica (~1.42) or that prepared by mixed of base and acid catalyzed silica (~1.34). On the other hand, the wavelength dispersions of the refractive index and extinction coefficient of pure VO_2 films below and above phase transition temperature were also measured and fitted by ellipsometry, which can be found from our previous work.[5]

Fig. 3(a) shows the XRD patterns of both bottom-layer and double-layer thin films on quartz substrates, including the standard pattern of monoclinic (M) VO_2 (PDF#82-0661). All the diffraction peaks of bottom-layer and double-layer films are similar, which correspond with the characteristic pattern of the VO_2 M-phase. It is worth noting that no other impurity peaks (such as V_2O_3, V_2O_5 or V_4O_9) can be observed in the XRD

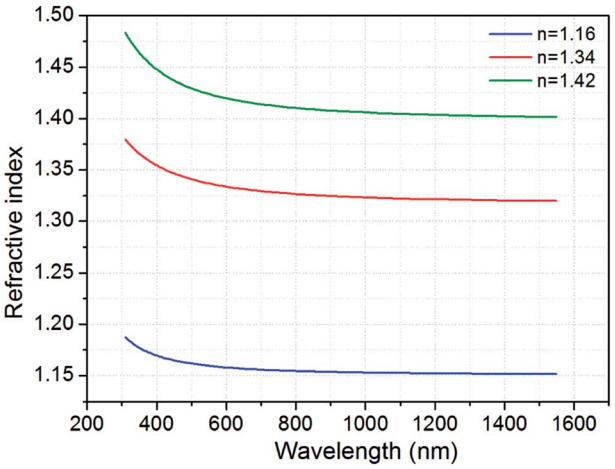

Fig. 2 Dispersion curves of the refractive indices of the SiO_2 AR coatings prepared on the fused quartz.

patterns, indicating the formation of high-purity single crystal VO_2 films. These reveal that high-quality VO_2 films were obtained through DC reactive magnetron sputtering at low substrate temperature and the crystalline of VO_2 in double-layer film was unchanged after coated with sol–gel silica antireflection coatings. Additionally, the broad peaks in the range of 10° to 25° were assigned to fused quartz substrates. The fine patterns of VO_2 (011) peaks is shown in Fig. 3(b). It can be obvious seen that the values of two film samples are both slightly smaller than 27.827° of VO_2 powder diffraction, and the value of intense diffraction peak position of the double-layer SiO_2/VO_2 film sample is slightly smaller than 27.805° of the pure VO_2 film sample. The stress in films could be calculated by the formula:[15]

$$\sigma = \frac{E}{2v}\frac{d_0 - d}{d_0} \quad (1)$$

where d and d_0 are the lattice distances in the strained and unstrained states, respectively. E and v are Young's modulus and Poisson's ratio of the film, respectively. The lattice coefficient could be obtained according to Bragg formula:

$$2d \sin\theta = k\lambda \quad (2)$$

where θ is the X-ray diffraction angle, and λ is the X-ray wavelength. The compressive stress in double-layer SiO_2/VO_2 film sample is larger than that of pure VO_2 film after calculation from the above formulas.

Fig. 4 shows the top-view SEM images of pure VO_2 and SiO_2/VO_2 bilayer films. For the pure VO_2 film, rice-like nanoparticles scattered on the surface, indicating the good crystallinity of the sample. The morphology is porous for the sample S116, while the sample S142 behaved a denser structure without any pores on the surface. The surface morphology of sample S134 shows both characteristic mentioned above. Moreover, the cross-sectional SEM image of sample S116 is shown in the inset image of Fig. 4, in which an obvious interface between the 110 nm SiO_2 antireflective layer and 150 nm VO_2 film can be observed.

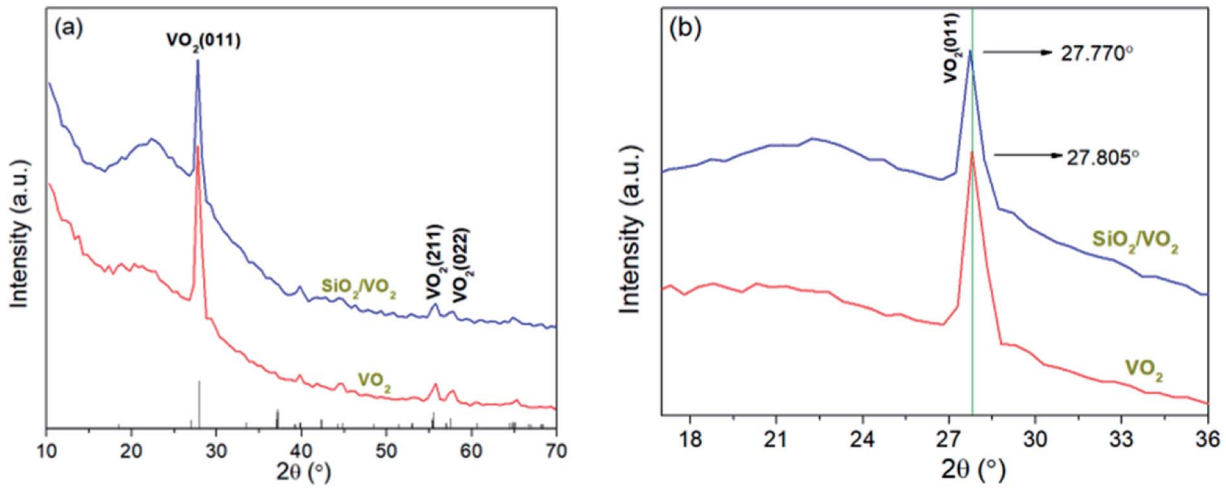

Fig. 3 XRD spectra of the pure VO_2 film and SiO_2/VO_2 film: (a) normalized patterns; (b) fine patterns of VO_2 (011) peaks.

Fig. 5(a) shows the temperature-dependent transmittance of the pure VO_2 film and S116 bilayer film sample at $\lambda = 1550$ nm. Thermal hysteresis loop is evident for both film samples and the semiconductor-to-metal transition occurred, indicating that the double-layer SiO_2/VO_2 film sample maintained the phase transition properties. Compared with the pure VO_2 film, the enhancement of transmittance at $\lambda = 1550$ nm is obvious, and the highest value can reach 72% for the sample S116. The tunable-RI SiO_2 coatings can significantly suppress the optical reflection losses and improve light transmission.

Fig. 5(b) shows the Standard Gauss fitting derivative logarithmic plots, which were obtained by taking the derivative of the logarithmic transmittance with respect to the temperature of film sample. Phase transition temperature can be defined as $T_c = (T_l + T_h)/2$, and the thermal hysteresis width was calculated by $\Delta H = T_h - T_l$. The values of phase transition temperatures for pure VO_2 and S116 film sample are 63.5 °C and 60 °C, respectively, which are lower than 68 °C of the bulk VO_2. Moreover, the phase transition temperature of sample S116 is lower than that of pure VO_2 film. The main reason is that the larger compressive

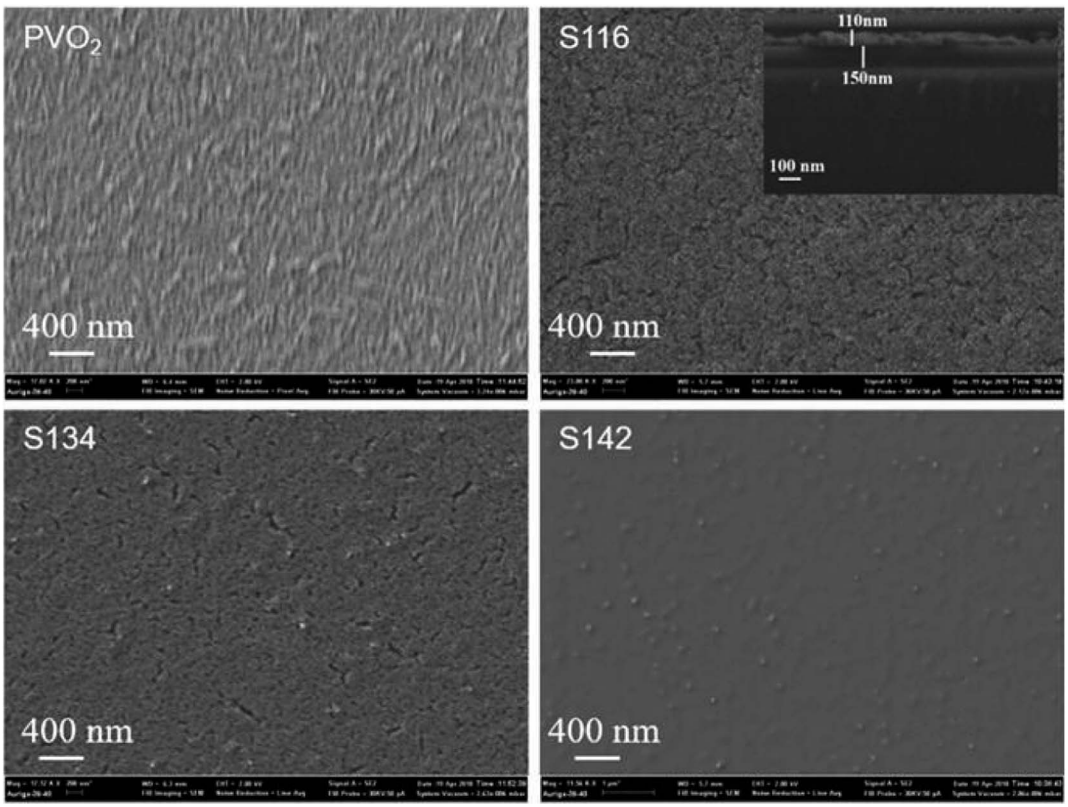

Fig. 4 Top-view SEM images of pure VO_2 and SiO_2/VO_2 bilayer films.

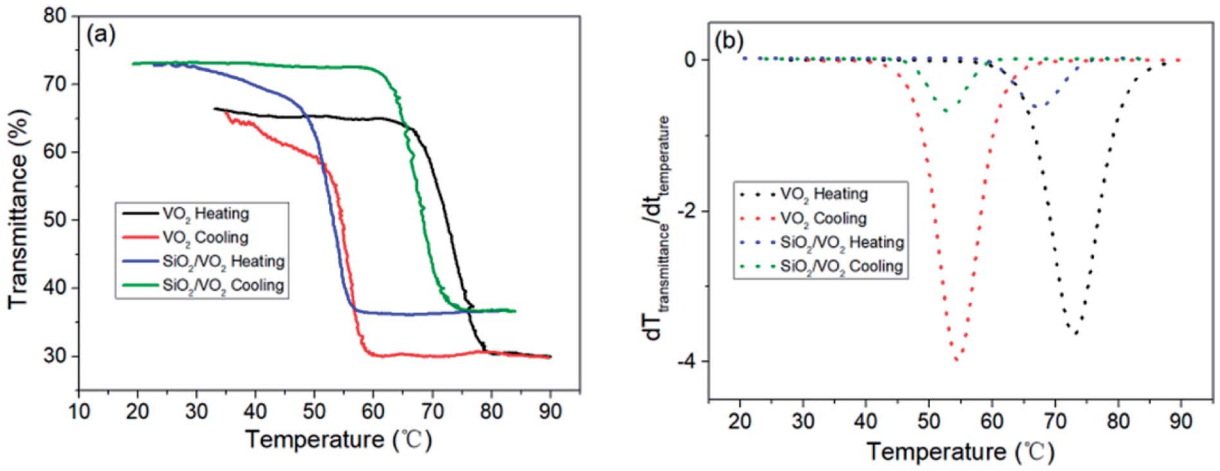

Fig. 5 (a) Transmittance hysteresis loops of pure VO_2 film and SiO_2/VO_2 bilayer films at $\lambda = 1550$ nm and (b) corresponding dT/dt *vs.* temperature curve for film samples PVO_2 and S116.

stress existed in the double-layer film sample compared with the pure VO_2 film sample, which has been discussed in the XRD analysis. Our previous work[32] reported that the compressive stress changed the phase transition temperature of VO_2 film samples by applying TiO_2 buffer layers. The width of the hysteresis loop of sample S116 is 14.5 °C, which is also smaller than that of pure VO_2 film sample (18.5 °C). These results are different from other reports, which usually revealed that adding SiO_2 antireflection coatings would increase the T_c and ΔH to a certain extent due to the existence of SiO_2 as thermal insulation.[24,28] The main reason of our experimental results may be the special porous morphology for the sample S116 with low refractive index.

To investigate the effect of RI-fixed SiO_2 coatings on the optical properties of the VO_2 films, the transmittance spectra were examined as shown in Fig. 6(a). The visible transmittance (at $\lambda = 700$ nm) and IR transmittance modulation (at $\lambda = 2500$ nm) of the film samples were calculated, as shown in Fig. 6(b). The transmittance at $\lambda = 700$ nm for the samples with SiO_2 antireflection coatings is higher than that of the single-layer VO_2 film, in which the sample with SiO_2 refractive index of 1.42 behaved the best. The visible transmittance at $\lambda = 700$ nm increased from 47% to 66% as the refractive index of SiO_2 antireflection coating increased from 1.16 to 1.42.

To fully display the superior optical properties of single-layer VO_2 and SiO_2/VO_2 double-layer films, the luminous transmittance (T_{lum}) and solar spectral transmittance (T_{sol}) of film samples were calculated based on the measured transmittance using the following eqn (3) and (4):

$$T_{sol} = \int \varphi_{sol}(\lambda)T(\lambda)d\lambda \Big/ \int \varphi_{sol}(\lambda)d\lambda \quad (3)$$

$$T_{lum} = \int \varphi_{lum}(\lambda)T(\lambda)d\lambda \Big/ \int \varphi_{lum}(\lambda)d\lambda \quad (4)$$

here, $T(\lambda)$ represents the transmittance, φ_{sol} is the solar spectral irradiance for mass of 1.5. The angle between the sun and the horizon is above 37° and the wavelength is 280–2500 nm. φ_{lum} is the standard luminous efficiency function of photonic vision and the wavelength for the φ_{lum} is 380–780 nm. The values of ΔT_{sol} and $T_{lum(avg)}$ can be obtained as follows:

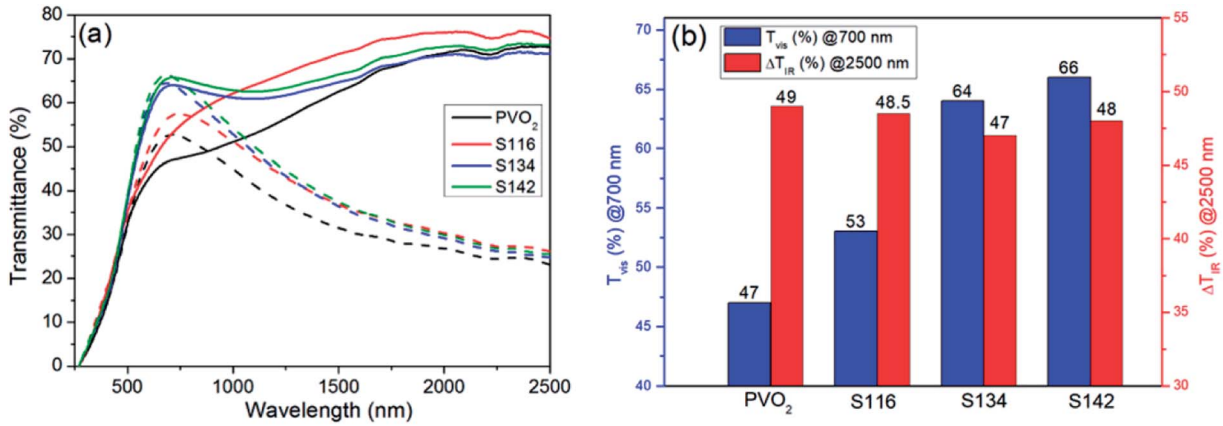

Fig. 6 (a)Transmittance spectra of pure VO_2 film and bilayer films. Solid lines represent the transmittance recorded at 25 °C and dotted lines measured at 80 °C. (b) T_{vis} at $\lambda = 700$ nm and ΔT_{IR} at $\lambda = 2500$ nm for the samples.

Table 1 Solar switching efficiency (ΔT_{sol}) and luminous transmittance (T_{lum}) of the pure VO_2 film and SiO_2/VO_2 bilayer films compared with the reported studies

Samples	$T_{sol,l}$ [%]	$T_{sol,h}$ [%]	ΔT_{sol} [%]	$T_{lum,l}$ [%]	$T_{lum,h}$ [%]	$T_{lum(avg)}$ [%]	ΔT_{lum} [%]
PVO_2 (this work)	44.57	38.32	6.25	37.06	40.10	38.58	3.04
S116 (this work)	50.71	42.43	8.28	40.81	43.04	41.93	2.23
S134 (this work)	54.14	45.99	8.15	47.77	48.37	48.07	0.60
S142 (this work)	**57.83**	**49.32**	**8.51**	**50.11**	**50.76**	**50.44**	**0.65**
VO_2@SiO_2 arrays[26]	—	—	6.70	—	—	43.50	—
SiO_2/VO_2 (ref. 27)	—	—	7.62	—	—	47.70	—
α-$SiO_2/VO_2/\alpha$-SiO_2 (ref. 33)	36.50	32.00	4.50	35.20	34.80	35.00	0.40
TiO_2/VO_2 (ref. 34)	46.25	39.26	6.99	49.15	45.05	47.10	4.10
TiO_2(R)/VO_2(M)/TiO_2(A)[35]	33.80	23.60	10.20	30.10	27.80	28.95	2.30
Moth-eye structure[20]	52.10	45.00	7.10	43.60	45.30	44.50	−1.70
$VO_2/SiO_2/TiO_2$ coating[36]	28.83	13.55	15.29	17.81	18.23	18.02	−0.42

$$\Delta T_{sol} = T_{sol,l} - T_{sol,h} \quad (5)$$

$$T_{lum(avg)} = (T_{lum,l} + T_{lum,h})/2 \quad (6)$$

here, $T_{sol,l}$ indicates the solar transmittance in semiconductor state and $T_{sol,h}$ indicates the solar transmittance in metal state. $T_{lum,l}$ and $T_{lum,h}$ mean the luminous transmittance in the low temperature state and high temperature state, respectively.

The solar switching efficiency (ΔT_{sol}) and visible transmittance (T_{lum}) of the pure VO_2 film and bilayer films are shown on Table 1. It is obvious that T_{lum} and ΔT_{sol} of the SiO_2/VO_2 films were all higher than the pure VO_2 film. Furthermore, the $T_{lum,l}$ and $T_{lum,h}$ of these samples both increased obviously as the refractive indices of SiO_2 coatings increased from 1.16 to 1.42, and the values of ΔT_{sol} also exhibited a slightly increasing trend at the same time. The maximum values of T_{lum} and ΔT_{sol} for film sample S142 can reach 50.44% and 8.51%, respectively. This result was better than the values of reported VO_2@SiO_2 arrays prepared by rapid thermal annealing of sputtered vanadium films,[26] SiO_2/VO_2 double-layered films obtained vis plasma enhanced chemical vapor deposition,[27] α-$SiO_2/VO_2/\alpha$-SiO_2 multi-layered films and TiO_2/VO_2 films deposited by radio frequency reactive magnetron sputtering.[33,34] Although the TiO_2(R)/VO_2(M)/TiO_2(A)[35] multi-layered films made through radio frequency reactive magnetron sputtering and $VO_2/SiO_2/TiO_2$ (ref. 36) films fabricated vis atmospheric-pressure chemical vapor deposition behaved higher ΔT_{sol} than our result, the values of their $T_{lum(avg)}$ were lower. More detailed results about recent studies were summarized in Table 1. In this work, the formation of smoother and denser film surface after SiO_2 coating can decrease the light scattering of the sample and enhance the visible transmittance. These results indicate that applying SiO_2 antireflection coatings with tunable refraction index can be an efficient way to enhance the visible transmittance of VO_2 films simultaneously and continuously.

4. Conclusion

In this work, SiO_2/VO_2 bilayer films were synthesized successfully by magnetron sputtering and sol–gel method. The crystallization properties of VO_2 films is essentially unchanged by applying SiO_2 top layer. The bilayer films can behave high transmittance and good thermochromic performance when compared with the single-layer pure VO_2 film. For the sample S142, the maximum value of T_{lum} can reach 50.44%. For the sample S116, the width of hysteresis loop and transition temperature are 14.5 °C and 60 °C, respectively, which are smaller than those of pure VO_2 film sample (18.5 °C and 63.5 °C). Moreover, the T_{lum} of these bilayer films increased obviously as the refractive index of SiO_2 antireflective layer increased from 1.16 to 1.42, and the ΔT_{sol} exhibited a slightly increasing trend. Hence, the enhancement of T_{lum} and ΔT_{sol} simultaneously and continuously provides a meaningful solution for VO_2-based thermochromic energy-efficient smart windows.

Conflicts of interest

There are no conflicts to declare.

Acknowledgements

This work was supported by the Shenzhen Science & Technology Project (JCYJ20150529164656098, ZDSY20170228105421966), National Nature Science Foundation of China (Grant No. 11705259) and the Research & Development Fund of Guangdong/ Shenzhen (2016B090930011, JCYJ20160226192609015).

References

1 Z. Y. Cao, Y. Lu, X. D. Xiao, Y. J. Zhan, H. L. Cheng and G. Xu, *Mater. Lett.*, 2017, **209**, 609–612.
2 J. B. Kana Kana, G. Vignaud, A. Gibaud and M. Maaza, *Opt. Mater.*, 2016, **54**, 165–169.
3 L. L. Fan, X. Q. Wang, F. Wang, Q. F. Zhang, L. Zhu, Q. Q. Meng, B. l. Wang, Z. M. Zhang and C. W. Zou, *RSC Adv.*, 2018, **8**, 19151–19156.
4 H. Y. Xu, Y. H. Huang, S. Liu, K. W. Xu, F. Ma and P. K. Chu, *RSC Adv.*, 2016, **6**, 79383–79388.
5 D. P. Zhang, M. D. Zhu, Y. Liu, K. Yang, G. X. Liang, Z. H. H. Zheng and X. M. Cai, *J. Alloys Compd.*, 2016, **659**, 198–202.

6 S. Chen, L. Dai, J. J. Liu, Y. F. Gao, X. L. Liu, Z. Chen, J. D. Zhou, C. X. Cao, P. G. Han, H. J. Luo and M. Kanahira, *Phys. Chem. Chem. Phys.*, 2013, **15**, 17537.
7 S. H. Chen, H. Ma, X. J. Yi, T. Xiong, H. C. Wang and C. J. Ke, *Sens. Actuators, A*, 2004, **115**, 28–31.
8 G. V. Jorgenson and J. C. Lee, *Sol. Energy Mater.*, 1986, **14**, 205.
9 J. Wu, W. X. Huang, Q. W. Shi, J. H. Cai, D. Zhao, Y. B. Zhang and J. Z. Yan, *Appl. Surf. Sci.*, 2013, **268**, 556–560.
10 K. Martens, I. P. Radu, S. Mertens, X. Shi, L. Nyns, S. Cosemans, P. Favia, H. Bender, T. Conard, M. Schaekers, S. De Gendt, V. Afanas'ev, J. A. Kittl, M. Heyns and M. Jurczak, *J. Appl. Phys.*, 2012, **112**, 124501.
11 V. Thery, A. Boulle, A. Crunteanu, J. C. Orlianges, A. Beaumont, R. Mayet, A. Mennai, F. Cosset, A. Bessaudou and M. Fabert, *J. Appl. Phys.*, 2017, **121**, 055303.
12 D. Vernardou, D. Louloudakis, E. Spanakis, N. Katsarakis and E. Koudoumas, *Sol. Energy Mater. Sol. Cells*, 2014, **128**, 36–40.
13 J. Sakai, M. Zaghrioui, V. T. Phuoc, S. Roger, C. Autret-Lambert and K. Okimura, *J. Appl. Phys.*, 2013, **113**, 123503.
14 Y. Huang, D. P. Zhang, Y. Liu, J. C. Jin, Y. Yang, T. Chen, H. Guan, P. Fan and W. Z. Lv, *Appl. Surf. Sci.*, 2018, **456**, 545–551.
15 M. D. Zhu, H. J. Qi, C. Li, B. Wang, H. Wang, T. R. Guan and D. P. Zhang, *Appl. Surf. Sci.*, 2018, **453**, 23–30.
16 M. D. Zhu, H. J. Qi, B. Wang, H. Wang, T. R. Guan and D. P. Zhang, *J. Alloys Compd.*, 2018, **740**, 844–851.
17 J. D. Zhou, Y. F. Gao, X. L. Liu, Z. Chen, L. Dai, C. X. Cao, H. J. Luo, M. Kanahira, C. Sun and L. M. Yan, *Phys. Chem. Chem. Phys.*, 2013, **15**, 7505.
18 N. R. Mlyuka, G. A. Niklasson and C. G. Granqvist, *Sol. Energy Mater. Sol. Cells*, 2009, **93**, 1685–1687.
19 L. T. Kang, Y. F. Gao, H. J. Luo, Z. Chen, J. Du and Z. T. Zhang, *ACS Appl. Mater. Interfaces*, 2011, **3**, 135–138.
20 X. K. Qian, N. Wang, Y. F. Li, J. H. Zhang, Z. C. Xu and Y. Long, *Langmuir*, 2014, **30**, 10766–10771.
21 Y. Ke, I. Balin, N. Wang, Q. Lu, A. I. Y. Tok, T. J. White, S. Magdassi, I. Abdulhalim and Y. Long, *ACS Appl. Mater. Interfaces*, 2016, **8**, 33112–33120.
22 Y. J. Ke, X. L. Wen, D. Y. Zhao, R. C. Che, Q. H. Xiong and Y. Long, *ACS Nano*, 2017, **11**, 7542–7551.
23 C. Liu, Y. Long, S. Magdassi and D. Mandler, *Nanoscale*, 2017, **9**, 485.
24 C. Wang, L. Zhao, Z. Liang, B. Dong, L. Wan and S. Wang, *Sci. Technol. Adv. Mater.*, 2017, **18**, 563–573.
25 D. Li, Y. Shan, F. Huang and S. Ding, *Appl. Surf. Sci.*, 2014, **317**, 160–166.
26 L. W. Zhou, J. R. Liang, M. Hu, P. Li, X. L. Song, Y. R. Zhao and X. Y. Qiang, *Appl. Phys. Lett.*, 2017, **110**, 193901.
27 J. H. Yu, S. H. Nam, J. W. Lee and J. H. Boo, *Materials*, 2016, **9**, 556.
28 J. Zhang, J. Wang, C. M. Yang, H. B. Jia, X. M. Cui and S. C. Zhao, *Sol. Energy Mater. Sol. Cells*, 2017, **162**, 134–141.
29 C. Liu, S. C. Wang, Y. Zhou, H. B. Yang, Q. Lu, D. Mandler, S. Magdassi, C. Y. Tay and Y. Long, *J. Alloys Compd.*, 2018, **731**, 1197–1207.
30 B. Shen, H. Y. Li, H. Xiong, X. Zhang and Y. X. Tang, *Chin. Opt. Lett.*, 2016, **14**, 083101.
31 Q. Jia, *Acta Opt. Sin.*, 2004, **24**, 65.
32 D. P. Zhang, K. Yang, Y. Li, Y. Liu, M. D. Zhu, A. H. Zhong, X. M. Cai, P. Fan and W. Z. Lv, *J. Alloys Compd.*, 2016, **684**, 719–725.
33 H. Kakiuchida, P. Jin and M. Tazawa, *Sol. Energy Mater. Sol. Cells*, 2008, **92**, 1279–1284.
34 P. Jin, G. Xu, M. Tazawa and K. Yoshimura, *Jpn. J. Appl. Phys.*, 2002, **41**, L278–L280.
35 J. Zheng, S. Bao and P. Jin, *Nano Energy*, 2015, **11**, 136–145.
36 M. J. Powell, R. Quesada-Cabrera, A. Taylor, D. Teixeira, I. Papakonstantinou, R. G. Palgrave, G. Sankar and I. P. Parkin, *Chem. Mater.*, 2016, **28**, 1369–1376.